PHOTONICS Research

Multi-mode microcavity frequency engineering through a shifted grating in a photonic crystal ring

Xiyuan Lu,[1,2,3] Yi Sun,[1,2] Ashish Chanana,[1] Usman A. Javid,[1,2] Marcelo Davanco,[1] and Kartik Srinivasan[1,2,*]

[1]Microsystems and Nanotechnology Division, Physical Measurement Laboratory, National Institute of Standards and Technology, Gaithersburg, Maryland 20899, USA
[2]Joint Quantum Institute, NIST/University of Maryland, College Park, Maryland 20742, USA
[3]e-mail: xiyuan.lu@nist.gov
*Corresponding author: kartik.srinivasan@nist.gov

Received 21 July 2023; revised 29 August 2023; accepted 30 August 2023; posted 31 August 2023 (Doc. ID 500375); published 26 October 2023

Frequency engineering of whispering-gallery resonances is essential in microcavity nonlinear optics. The key is to control the frequencies of the cavity modes involved in the underlying nonlinear optical process to satisfy its energy conservation criterion. Compared to the conventional method that tailors dispersion by cross-sectional geometry, thereby impacting all cavity mode frequencies, grating-assisted microring cavities, often termed as photonic crystal microrings, provide more enabling capabilities through mode-selective frequency control. For example, a simple single period grating added to a microring has been used for single frequency engineering in Kerr optical parametric oscillation (OPO) and frequency combs. Recently, this approach has been extended to multi-frequency engineering by using multi-period grating functions, but at the cost of increasingly complex grating profiles that require challenging fabrication. Here, we demonstrate a simple approach, which we term as shifted grating multiple mode splitting (SGMMS), where spatial displacement of a single period grating imprinted on the inner boundary of the microring creates a rotational asymmetry that frequency splits multiple adjacent cavity modes. This approach is easy to implement and presents no additional fabrication challenges compared to an unshifted grating, and yet is very powerful in providing multi-frequency engineering functionality for nonlinear optics. We showcase an example where SGMMS enables OPO across a wide range of pump wavelengths in a normal-dispersion device that otherwise would not support OPO.

https://doi.org/10.1364/PRJ.500375

1. INTRODUCTION

Nanophotonic platforms have enabled a wide variety of applications in optical systems engineering. One major advantage of these platforms is their capability to achieve complex functionality by photonic integrated circuits [1,2], which is often enabled by the precise control over the effective refractive index of the waveguides. Particularly in nonlinear optics, nanophotonic devices can enable phase matching of many nonlinear optical interactions that are challenging in bulk materials [3] or fiber [4]. Generally, this is done by superimposing geometrical dispersion on the nanophotonic waveguide to compensate for material dispersion [5]. In this regard, the whispering-gallery-mode (WGM) resonator has been the workhorse geometry among all optical microcavities [6] for a wide variety of optical processes, including nonlinear optical interactions, optical sensing, and gain media for lasing [7–9]. These cavities provide tight confinement of light with high quality factors, resulting in an enhanced spatial and temporal enhancement for the intensity of the light field, which drives the efficiency of nonlinear optical processes [3]; however, they impose strict constraints on frequency and phase matching by requiring the interacting modes to have specific azimuthal mode orders and resonance frequencies to satisfy angular momentum and energy conservation, respectively. Such criteria have been satisfied, for example, in the application of chip-integrated WGM resonators to a wide variety of $\chi^{(2)}$ and $\chi^{(3)}$ nonlinear processes such as optical parametric oscillation (OPO) [10–15] and frequency comb generation [16,17]. In these cavities, dispersion can be engineered by tuning the geometrical parameters, i.e., the thickness, width, or radius of the ring. This technique, however, can control dispersion only globally, with the resonance frequency of every mode of the ring being impacted.

Another dispersion-engineering technique uses sinusoidal modulation of the WGM resonator width to create backscattering for a targeted mode [18]. This technique, referred to here

as selective mode splitting (SMS), can create sharp changes to dispersion at very specific wavelengths, where the resonator modes traveling clockwise (CW) and counterclockwise (CCW) have the correct momentum to be coupled by such coherent scattering induced by the grating modulation. The coupling strength is manifested in the splitting of the mode frequencies, as illustrated in Fig. 1(a). Here, the backscattering can induce a mode-selective change to dispersion by causing the resonance to split into a doublet, shifting its frequency. This can be used to phase-match nonlinear interactions that otherwise would be mismatched in frequency [19–22], where the width-modulated WGM resonator is also referred to as a photonic crystal ring. The SMS approach can be extended to multiple modes by a simple sum of different modulation frequencies, each of which targets a specific mode, termed multiple SMS [23], as illustrated in Fig. 1(b). This approach has recently been extended through Fourier synthesis to generate spatial domain modulation functions that target a large number of modes for broader-band applications [24], as illustrated in Fig. 1(c). Alternatively, one can also consider inverse design [25,26] to scatter specific momentum modes by a desired amount. These techniques [24–26], though meticulous in their analysis, can produce spatial modulation functions that may be complex to implement, posing challenges in device design, fabrication, and the optical quality of the resonances.

In this paper, we introduce a simplified design approach to control dispersion of multiple modes using just a single modulation frequency. We will refer to this method as the shifted grating multiple mode splitting (SGMMS). This approach is illustrated in Fig. 1(c), where we create an offset in the center of the spatial modulation of the ring width. In this technique, the modulation frequency targets a specific mode, as earlier, but the magnitude of the radial offset can control the number of modes that are split in frequency (when the offset is zero, only the targeted mode is split). Therefore, a larger offset can induce mode splitting of multiple modes without use of a complex multi-frequency modulation function. We demonstrate the capability of this technique by simulating and experimentally demonstrating an optical parametric oscillator (OPO) in a silicon nitride ring resonator whose output colors are tuned by

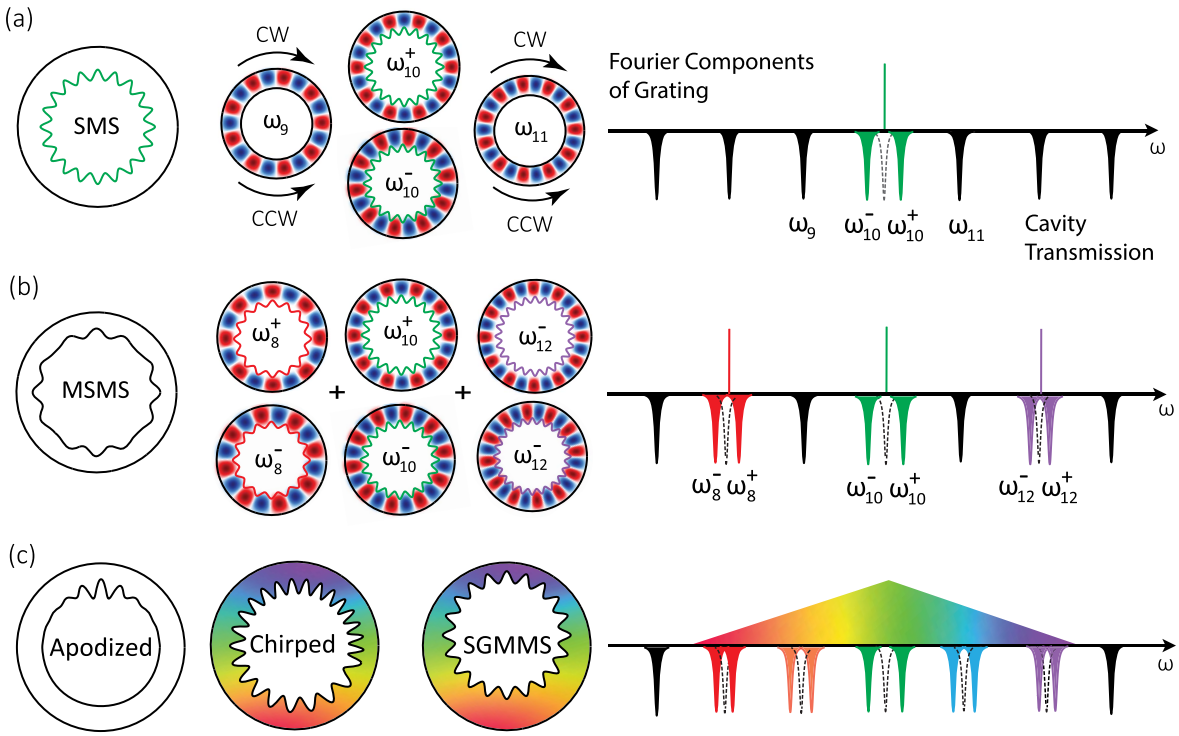

Fig. 1. Illustration of past techniques using grating-assisted microrings for frequency engineering and the current approach of shifted grating multiple mode splitting (SGMMS). (a) In the single frequency engineering case, a simple sinusoidal modulation of the inner boundary of the ring causes one mode, whose number of modulation periods is twice the m number, to have its resonance frequency split into two. Other modes that are not matched can remain in their clockwise (CW) and counterclockwise (CCW) traveling-wave propagation, and have no splitting in general. This process is termed selective mode splitting [18], as illustrated in the right panel of (a). Fourier analysis of the grating spatial frequency produces a delta function at the selected mode, and the microring cavity transmission displays that only the targeted mode is split. (b) Selective mode splitting can be extended to multi-frequency engineering by a simple sum of different spatial frequencies, termed as multiple selective mode splitting (MSMS) [23], with the corresponding Fourier components and device transmission shown on the right. (c) An apodized or chirped grating, with more detailed Fourier analysis [24] or inverse design [26], can yield a continuous modulation of grating spatial frequencies, with the splitting amplitudes typically varying in a continuous function versus mode frequencies. The shape of the grating profiles can be nontrivial to design and fabricate. We propose to circumvent these issues by using a simple single frequency sinusoidal grating with an offset shifted from the ring center. The SGMMS technique can introduce controlled mode splitting in multiple modes by an intuitive design. We note that the displayed triangular function for the spectral profile of the mode splitting is for illustration purpose only, and generally speaking, one can have various line shapes depending on the specific grating parameters in use.

adjusting which of the SGMMS modes is pumped. We show how several different pump modes from the same device, with a normal dispersion around the pump, can simultaneously phase- and frequency-match the OPO interaction. In total, we find that the SGMMS technique offers a simplified design approach for dispersion control over multiple modes that is robust to fabrication constraints and maintains high optical quality factors. We anticipate that it can be applied to phase- and frequency-match any cavity-enhanced parametric nonlinear optical processes.

2. PRINCIPAL IDEA

Grating technology, including not only uniform structures but also apodized and chirped geometries, has existed for decades, and specific implementations, such as fiber Bragg gratings, have been widely used in sensing, filtering, and lasing [27]. The topic discussed here, a grating inscribed in a microring, has also been studied in many contexts. Some studies have focused on optical filtering, including for laser applications [28–30], while others have examined ejection into free-space orbital angular momentum (OAM) states [31], for example, in frequency comb applications [32,33], where spectral control across multiple modes is also relevant [24,25]. As the grating modulation strength increases, concepts from photonic crystals are increasingly involved, and indeed, photonic crystal microrings (PhCRs) exhibiting slow light and defect-mode localization [34,35] have been demonstrated. Here, we focus our study of SGMMS for multi-frequency engineering in a regime where a perturbative single-frequency grating is imprinted upon a microring with a large and slow variation of its ring width.

The context of SGMMS follows that of SMS [18]. For instance, the ring width shown in Fig. 1(a) is modulated with 20 periods per circumference targeting the optical mode with an azimuthal mode number of 10. This modulation results in coupling between the CW and CCW modes, breaking their frequency degeneracy. Consequently, two new standing-wave modes emerge at up-shifted and down-shifted frequencies, as illustrated by two mode profiles labeled ω_{10}^{+} and ω_{10}^{-} in Fig. 1(a). The magnitude of the mode splitting $2\beta_{10}$, representing the frequency difference between the two modes, depends on the amplitude of the geometric modulation applied at the corresponding angular frequency (A_{20}). By precisely adjusting the modulation amplitude, the cavity frequencies can be accurately controlled. Additionally, when $m \neq 10$, where the modulation is out of phase with the optical mode, the optical mode remains unperturbed. For example, the ω_9 and ω_{11} modes are unperturbed by SMS and effectively see only the average microring. This orthonormal property forms the basis of grating-assisted frequency engineering [18,23,24,26], and can be understood through perturbation theory of optical modes with shifted boundaries [36], with

$$\beta_m = \frac{\omega_m}{2}\frac{\int \mathrm{d}S \cdot A[(\epsilon_c - 1)|E_{||}|^2 + (1 - 1/\epsilon_c)|D_{\perp}|^2]}{\int \mathrm{d}V \epsilon(|E_{||}|^2 + |E_{\perp}|^2)}, \quad (1)$$

where $E_{||}$ ($D_{||}$) and $E_{\perp}$ ($D_{\perp}$) are the electric field components (displacement field components) of the unperturbed optical mode polarizations that are parallel (||) and perpendicular ($\perp$) to the modulation boundary dS, respectively. ϵ represents the dielectric function of the material, including the silicon nitride core ($\epsilon = \epsilon_c$), silicon dioxide substrate, and air cladding ($\epsilon = 1$).

When considering either transverse electric (TE)-field-like modes or transverse magnetic (TM)-field-like modes, the previous equation can be simplified even further. This simplification arises due to the dominance of the term involving either $D_{\perp}$ or $E_{||}$ in the numerator's integral. Consider TE-like modes as an example, where the modulation of the ring width for SGMMS is given by

$$W(\phi) = W_0 + A_1 \cos(\phi) + A_{2m} \cos(2m\phi). \quad (2)$$

This SGMMS microring is illustrated by the third schematic in Fig. 1(c). The azimuthal angle ϕ is illustrated in Fig. 2(a).

When A_1 is perturbative, it has no effect on β_m. The standing-wave mode with a larger frequency has a dominant displacement field $D(r, \phi, z) = D(r, z)\cos(m\phi)$, and Eqs. (1) and (2) lead to

$$\beta_m = \frac{A_{2m}\omega_m}{2}\frac{\int \mathrm{d}S(1 - 1/\epsilon_c)|D(r,z)|^2 \cos^2(m\phi)\cos(2m\phi)}{\int \mathrm{d}V\epsilon(|E_z|^2 + |E_\phi|^2 + |E_r|^2)\cos^2(m\phi)}.$$

Here the azimuthal part can be integrated separately:

$$\beta_m = g_m A_{2m}/2, \quad (3)$$

where g_m is defined as

$$g_m \equiv \frac{\omega_m}{2}\frac{\int \mathrm{d}S(1 - 1/\epsilon_c)|D(r,z)|^2}{\int \mathrm{d}V\epsilon(|E_z|^2 + |E_\phi|^2 + |E_r|^2)}. \quad (4)$$

This linear dependence of mode splitting on modulation amplitude holds only in the perturbative regime. A counterintuitive observation is that the mode splitting can vanish to zero when the modulation amplitude increases to a critical value [24,25], and this effect can occur regardless of the grating shape (sinusoidal, square, etc.) or photonic layer structure (cladding type, cladding symmetry, etc.) [37]. Such "bandgap closing" introduces additional complication when designing apodized gratings in microrings [24]. In this work, we restrict our analysis to the perturbative regime, where the mode splitting (bandgap) has a monotonic and linear dependence on modulation amplitude, to avoid this complication.

In the SGMMS case, when the slow-variation term $A_1 = S/2$ is small (where S is the shift relative to the center of the microring outside boundary), the splitting observed is expected to be close to the SMS case, with only a small amount of decreased mode splitting. When A_1 is large, for example, the narrowest and widest parts of rings correspond to resonance frequencies over multiple free-spectral ranges, and other adjacent modes will also exhibit mode splittings. Instead of an integration with ϕ from 0 to 2π, only a subset of this integration range close to the targeted frequency would be relevant:

$$\beta_n \approx \frac{\Delta\phi_n}{2\pi}\frac{g_m A_{2m}}{2}, \quad (5)$$

where $2m$ is the number of modulation periods within the ring circumference, and n is the mode under consideration. We notice from Eq. (5) that the shifted-grating microring resembles a chirped-grating microring [27], as illustrated in Fig. 1(c). The range of modes with splittings, that is, the range of n with considerable β, is decided by the narrowest and widest ring

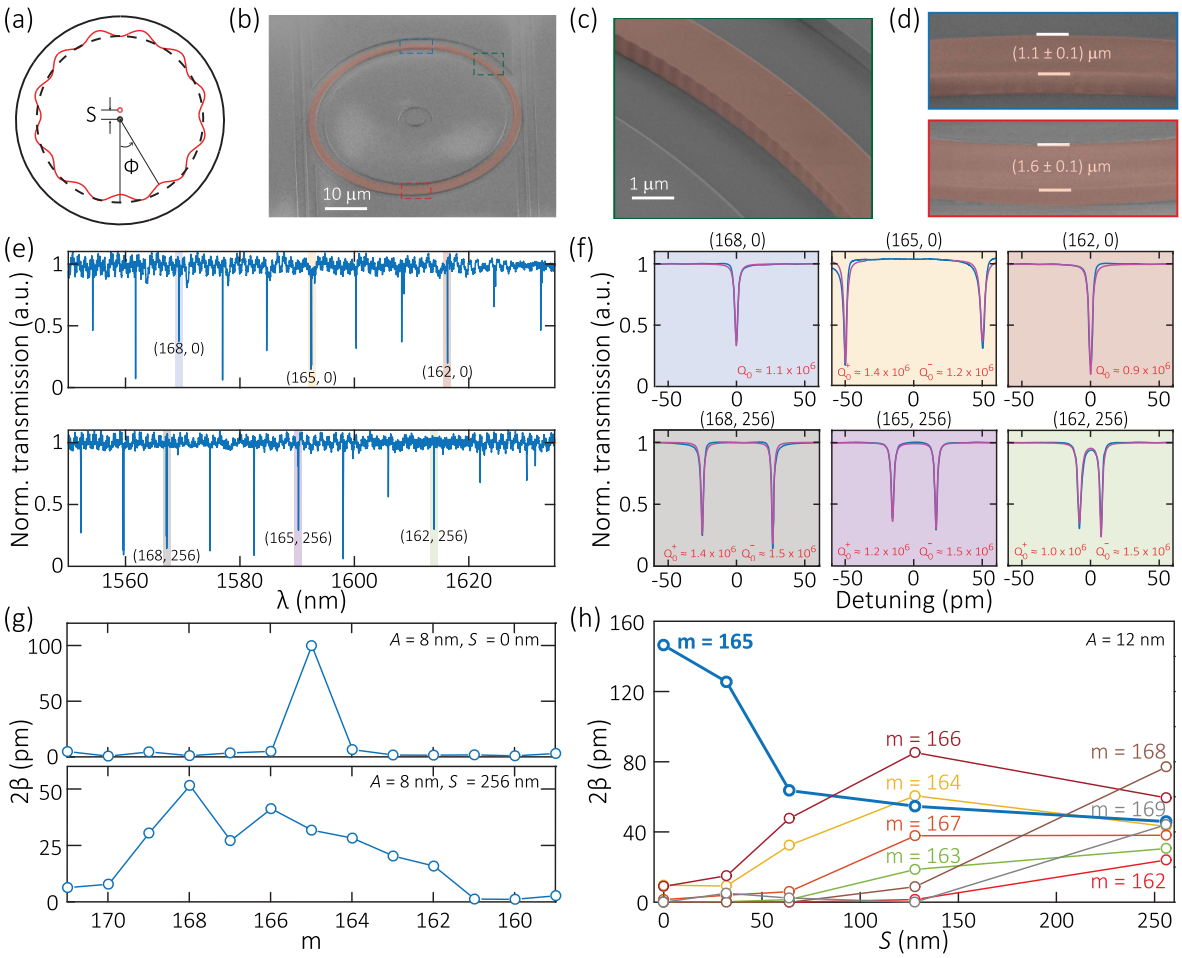

Fig. 2. Experimental demonstration of SGMMS. (a) Illustration of the SGMMS device with upward-shifted grating. The red and black circles indicate the centers of the inside boundary (i.e., the shifted grating) and the outside boundary of the microring, respectively. (b) Scanning electron microscope (SEM) image of an SGMMS microring, false colored in red, with coupling waveguides on the left and right sides. In this paper, only the right waveguide is used in experiments. The grating has a nominal shift $S = 256$ nm. The nominal average ring width is RW $= 1.5$ μm. Zoom-in images of three parts of the microrings, highlighted by the dashed boxes, are shown in (c) and (d). (c) An SEM image of the microring shows a sinusoidal modulation with a nominal amplitude of $A = 12$ nm. (d) The narrowest and widest RWs are measured to be (1.1 ± 0.1) μm and (1.6 ± 0.1) μm, respectively, where the quoted uncertainty is the one standard deviation from multiple estimates from the SEM image. (e) Normalized transmission spectra for the SMS device (top panel) with $A = 8$ nm and $S = 0$ nm and the SGMMS device (bottom panel) with the same A but $S = 256$ nm. Labels (m, S) represent the azimuthal mode number and the shift in nanometers, respectively. (f) Scaled transmission spectra from (e) with annotations of the fitted Q values. In the top panel, the SMS device shows a mode splitting of approximately 100 pm only at $m = 165$ and negligible mode splittings at nearby modes. In the bottom panel, the SGMMS modulation introduces mode splittings across multiple modes. The mode splittings for $m = 168$, 165, and 162 are approximately 52, 32, and 16 pm, respectively. All these modes show high optical quality, with intrinsic Q around 10^6. (g) Summary of the measured mode splittings (2β) across all modes in (e). (h) Evolution of mode splittings from $S = 0$ nm to $S = 256$ nm, with a fixed $A = 12$ nm. Above $S = 50$ nm, adjacent modes increasingly start to show appreciable mode splittings. The uncertainties in mode splitting values in (g) and (h) are smaller than the data point size.

widths, which is straightforward to determine in simulation. The value of $\Delta\phi$ is not as easy to calculate accurately, though intuitively easy to connect to Fig. 1(c). We will measure the splittings experimentally in the next section.

3. EXPERIMENTAL VERIFICATION

We validate the SGMMS design using a high-intrinsic-quality-factor (Q) Si_3N_4/SiO_2 microring resonator platform from a standard fabrication process [38]. We implemented a grating modulation amplitude (A) on the inner side of the microring, with a shift (S) relative to the center of the outside boundary, as illustrated in Fig. 2(a). The fabricated device, shown in Figs. 2(b)–2(d), has a nominal outside ring radius, average ring width (RW), and Si_3N_4 thickness of 25 μm, 1500 nm, and 600 nm, respectively. This device has nominal $A = 12$ nm and $S = 256$ nm. This S can be confirmed by half of the differences between the narrowest and the widest ring widths, as shown in Fig. 2(d).

We compare the SMS and SGMMS devices in Figs. 2(e)–2(g), and more closely examine the details of multi-frequency engineering of SGMMS in Fig. 2(h). We first examine the

mode splitting behavior for the SMS device, that is, the control device for SGMMS (no shift). Here, we target the fundamental TE mode with $m = 165$, which has a resonance around 1592 nm. This device has $A = 8$ nm and $S = 0$ nm. The transmission spectrum of this device is shown in the top panel of Fig. 2(e). The mode splittings of this device at all modes are summarized in the top panel of Fig. 2(g), and it shows the typical behavior of an SMS device. There is only one notable mode splitting of approximately 100 pm at the targeted mode $m = 165$, and the mode splittings at nearby modes are all less than 10 pm and comparatively negligible, in agreement with previous reports [23].

We transform an SMS device into an SGMMS device by introducing the shift S. The bottom panel of Fig. 2(e) shows the transmission spectrum of a fabricated SGMMS device with the same $A = 8$ nm as the control SMS device and $S = 256$ nm. As the shift is increased from 0 to 256 nm, the mode splittings are spread from the central mode at $m = 165$ onto eight modes with varying mode splittings of approximately {30, 52, 27, 41, 32, 28, 20, 16} pm at $m = \{169, 168, 167, 166, 165, 164, 163, 162\}$, respectively, as shown in Fig. 2(g). One may also wonder if there is any negative effect on the optical quality factors with such large shift S. Previous works [18,34] have shown that a grating with large modulations does not degrade the optical quality factors. In this work, we show that adding a large shift to this grating also maintains the Q. The intrinsic Q maintain values over 1 million even with a shift $S = 256$ nm as shown in Fig. 2(f). We also investigate the behavior of the mode splitting with various S for another series of SGMMS devices with a fixed $A = 12$ nm. In general, the number of modes with appreciable splitting (e.g., >10 pm) increases with S, while the maximum splitting amplitude for any mode occurs at $S = 0$, where the entire effect of the grating is concentrated on one m. For example, the appreciable mode splittings are spread from the central mode to two additional modes when $S = 64$ nm, four additional modes when $S = 128$ nm, and eventually seven additional modes (eight modes in total) when $S = 256$ nm as shown in Fig. 2(h). Thus, the SGMMS approach introduces multiple frequency engineering capabilities with intuitive design and fabrication while maintaining high optical quality factors, all simply by adding a linear shift to an SMS device.

4. OPO APPLICATION

After validating the concept of SGMMS in the previous section, we now apply this technique directly to frequency engineering problems in nonlinear nanophotonics applications. One important application is OPO, which converts an input laser from one color (i.e., the pump) to two different output colors (i.e., the signal and idler). OPO with the pump in either the normal or anomalous dispersion regime is possible; we focus on the former, where the signal–idler separation can be particularly broad and devoid of extraneous spectral tones [10]. To realize such OPO, a close-to-zero but positive frequency mismatch $\Delta\nu = \nu_s + \nu_i - 2\nu_p$ is required, where $\nu_{p,s,i}$ are the pump, signal, and idler modes, respectively, as a result of the interplay between self- and cross-phase modulation of these three modes. The requisite frequency matching in a microring is typically realized through accurate cross-sectional geometric control, but this comes with two main disadvantages: (1) the device is very sensitive to the geometric dispersion, which puts stringent requirements in design and fabrication; and (2) the close-to-zero dispersion requires a device layer thickness that is much larger than that typically offered within fabrication facilities for passive silicon nitride photonic circuits. Such thicker films typically require some level of additional fabrication (e.g., stress mitigation or damascene processing) to mitigate stress [39], which in turn complicates integration of OPO into more complex systems.

The SMS approach has been applied to address the above challenges in previous works on OPO and frequency combs [19–22]. However, this prior approach enables OPO at the cost of constraining the pump laser to be at a specific wavelength (mode) defined by the SMS. Here, we employ the SGMMS approach to extend the number of available modes for the pump to enable OPO across the S + C + L bands (specifically from 1460 to 1625 nm).

To take advantage of the full scanning range of our measurement laser (from 1450 to 1650 nm), the SGMMS device characterized in Fig. 2 ($A = 12$ nm and $S = 256$ nm) is subsequently etched from 600 nm to 500 nm thickness, to shift the SGMMS central wavelength from 1592 nm to 1552 nm, per NIST requirements on units. Figure 3(a) shows the transmission spectrum of the etched device, with the corresponding mode splitting values summarized in Fig. 3(b). The SGMMS device shows a similar behavior as in Figs. 2(g) and 2(h), and there are 10 modes (from $m = 171$ to $m = 162$) showing notable mode splitting values after etching. Though this device has normal dispersion across the telecom, all the redshifted split modes can be pumped to generate OPO [19]. Figure 3(c) shows the experimental results of the OPO spectra as we pump six of these split modes. When pumped at the redshifted mode for $m = 165$ (the top panel), we get a wide signal–idler span of 134 nm, in agreement with the frequency mismatch diagram in the top panel of Fig. 3(d). This scheme is similar to prior SMS-OPO works, where the mode splitting was implemented for only one mode, either the pump [19,20] or the signal [21].

Next, we leverage the multi-mode character of the SGMMS technique, where we pump the split modes at different m numbers and observe OPO for all modes. Figure 3(c) shows the other five OPO spectra obtained when pumped at different modes accessible within our available amplifier range. For $m = 162$ (middle panel) and $m = 159$ (bottom panel), when pumped on the redshifted resonances, two signal–idler pairs are observed at the red-shifted resonances for $m = 162$ and at the blue-shifted resonances for $m = 159$. The data are in good agreement with the simulation and the measured frequency mismatch ($\Delta\nu/2$) as shown in the middle and bottom panels of Fig. 3(d), where the frequency dashed red line indicates the mode combinations that satisfy the OPO frequency matching condition. These two examples showcase the flexibility of the SGMMS approach in multi-frequency engineering. Such capability can advance the functionalities of other related nonlinear processes, including entangled photon-pair generation [38,40], quantum frequency conversion via four-wave-mixing Bragg scattering [41], and frequency comb generation.

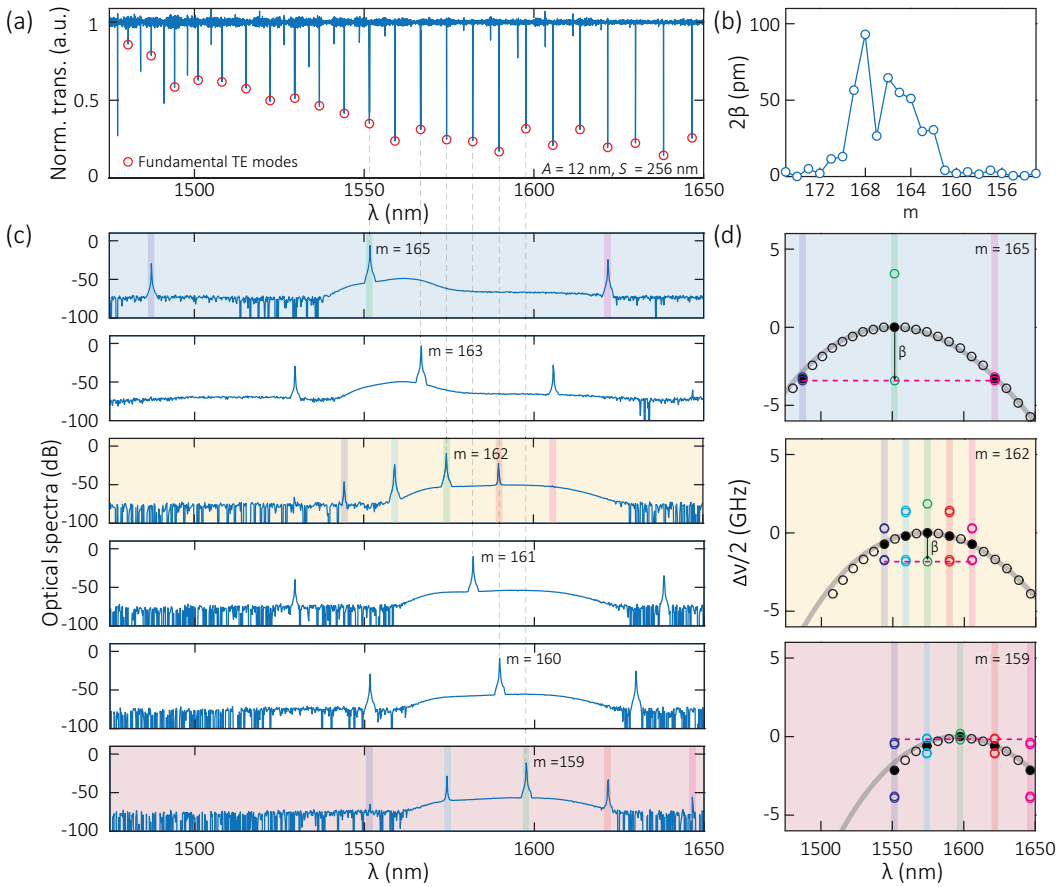

Fig. 3. Application of SGMMS for pump-mode-selectable optical parametric oscillation. (a) Transmission spectrum of a fabricated SGMMS device with $A = 12$ nm and $S = 256$ nm. The resonance dips for the fundamental TE modes are circled in red. The target SMS mode is near 1552 nm with $m = 165$. (b) Summary of the measured mode splitting values for the device in (a) from $m = 175$ to $m = 153$. With a shift $S = 256$ nm, there are 10 modes (from $m = 171$ to $m = 162$) with mode splitting values larger than 10 pm. (c) Optical spectra from a series of OPO experiments, where the pump mode is varied between any of the six split modes at $m = \{165, 163, 162, 161, 160, 159\}$. On the y axis, 0 dB is referenced to 1 mW, i.e., dBm. (d) Frequency mismatch diagrams when pumping at $m = \{165, 162, 159\}$. The gray curves are from finite-element-method simulations, and the circles are from experimental measurements. The uncertainties are smaller than the symbol size. The mode splittings for relevant mode numbers are illustrated in colored circles, while their central (un-split) frequencies are in solid black circles. Modes that are unrelated to the OPO process only have their central frequencies shown, in empty black circles. The frequency matching condition for OPO is achieved at the red dashed lines. The colored columns highlighting involved modes in both (c) and (d) are for guidance of viewing.

In photon-pair generation [24,26,42], this method eases the task of creating mode splitting of the pump mode while maintaining a high optical quality factor [38], which leads to CW and CCW path entanglement of signal and idler photon pairs [40]. In four-wave-mixing Bragg scattering, usage of the split mode for the pump laser can create the dispersion property required for quantum frequency conversion while also eliminating unwanted conversion channels [41]. In frequency comb generation, our method simplifies the design of photonic crystal rings for both dispersion engineering [24,26] and injection locking purposes [42].

5. DISCUSSION

In summary, we demonstrate a nanophotonic frequency engineering approach that we term as SGMMS, with controllable mode splittings across multiple resonator modes through a shifted, single frequency grating. SGMMS offers another level of simplicity in design and fabrication over existing approaches [23,24,26]. We further apply SGMMS-based frequency engineering to OPO across multiple pump modes in one microring device, with the generated signal and idler output frequencies dependent on the pumped mode. Such results cannot be achieved using the previously demonstrated single mode splitting devices [19,20] or through combinations of different (un-split) transverse mode families [43,44]. While well-engineered OPO devices without the introduction of mode splittings can also support OPO on multiple pump modes, they have a more stringent tolerance of only a few nanometers in cross-sectional geometry [10,13], a result of the requirement to balance normal dispersion near the pump with higher-order dispersion for frequency matching. More generally, we anticipate that the introduction of a shift in the grating position shown in this work can be combined with previous multiple-mode splitting

techniques [23,24] and other dispersion engineering approaches to extend microcavity frequency engineering capabilities for nonlinear optical processes.

Funding. Maryland Innovation Initiative; National Institute of Standards and Technology (NIST-on-a-chip); Defense Advanced Research Projects Agency (LUMOS).

Acknowledgment. X.L. acknowledges support from the Maryland Innovation Initiative.

Disclosures. X.L. and A.C. are the co-founders of LightSiNC NanoTech, LLC.

Data Availability. Data underlying the results presented in this paper are not publicly available at this time but may be obtained from the authors upon reasonable request.

REFERENCES

1. T. Koch and U. Koren, "Semiconductor photonic integrated circuits," IEEE J. Quantum Electron. **27**, 641–653 (1991).
2. R. Nagarajan, C. H. Joyner, R. P. Schneider, J. S. Bostak, T. Butrie, A. G. Dentai, V. G. Dominic, P. W. Evans, M. Kato, M. Kauffman, D. J. H. Lambert, S. K. Mathis, A. Mathur, R. H. Miles, M. L. Mitchell, M. J. Missey, S. Murthy, A. C. Nilsson, F. H. Peters, S. C. Pennypacker, J. L. Pleumeekers, R. A. Salvatore, R. K. Schlenker, R. B. Taylor, H.-S. Tsai, M. F. Van Leeuwen, J. Webjorn, M. Ziari, D. Perkins, J. Singh, S. G. Grubb, M. S. Reffle, D. G. Mehuys, F. A. Kish, and D. F. Welch, "Large-scale photonic integrated circuits," IEEE J. Sel. Top. Quantum Electron. **11**, 50–65 (2005).
3. R. W. Boyd, *Nonlinear Optics* (Academic, 2008).
4. G. Agrawal, *Nonlinear Fiber Optics* (Academic, 2007).
5. G. Agrawal, *Lightwave Technology: Components and Devices* (Wiley, 2004).
6. K. J. Vahala, "Optical microcavities," Nature **424**, 839–846 (2003).
7. V. Ilchenko and A. Matsko, "Optical resonators with whispering-gallery modes-part II: applications," IEEE J. Sel. Top. Quantum Electron. **12**, 15–32 (2006).
8. M. R. Foreman, J. D. Swaim, and F. Vollmer, "Whispering gallery mode sensors," Adv. Opt. Photonics **7**, 168–240 (2015).
9. S. Yang, Y. Wang, and H. Sun, "Advances and prospects for whispering gallery mode microcavities," Adv. Opt. Mater. **3**, 1136–1162 (2015).
10. X. Lu, G. Moille, A. Singh, Q. Li, D. A. Westly, A. Rao, S.-P. Yu, T. C. Briles, S. B. Papp, and K. Srinivasan, "Milliwatt-threshold visible-telecom optical parametric oscillation using silicon nanophotonics," Optica **6**, 1535–1541 (2019).
11. A. W. Bruch, X. Liu, J. B. Surya, C.-L. Zou, and H. X. Tang, "On-chip $\chi^{(2)}$ microring optical parametric oscillator," Optica **6**, 1361–1366 (2019).
12. T. P. McKenna, H. S. Stokowski, V. Ansari, J. Mishra, M. Jankowski, C. J. Sarabalis, J. F. Herrmann, C. Langrock, M. M. Fejer, and A. H. Safavi-Naeini, "Ultra-low-power second-order nonlinear optics on a chip," Nat. Commun. **13**, 4532 (2022).
13. X. Lu, G. Moille, A. Rao, D. A. Westly, and K. Srinivasan, "On-chip optical parametric oscillation into the visible: generating red, orange, yellow, and green from a near-infrared pump," Optica **7**, 1417–1425 (2020).
14. Y. Okawachi, M. Yu, J. K. Jang, X. Ji, Y. Zhao, B. Y. Kim, M. Lipson, and A. L. Gaeta, "Demonstration of chip-based coupled degenerate optical parametric oscillators for realizing a nanophotonic spin-glass," Nat. Commun. **11**, 4119 (2020).
15. C. Reimer, M. Kues, L. Caspani, B. Wetzel, P. Roztocki, M. Clerici, Y. Jestin, M. Ferrera, M. Peccianti, A. Pasquazi, B. E. Little, S. T. Chu, D. J. Moss, and R. Morandotti, "Cross-polarized photon-pair generation and bi-chromatically pumped optical parametric oscillation on a chip," Nat. Commun. **6**, 8236 (2015).
16. A. L. Gaeta, M. Lipson, and T. J. Kippenberg, "Photonic-chip-based frequency combs," Nat. Photonics **13**, 158–169 (2019).
17. L. Chang, S. Liu, and J. E. Bowers, "Integrated optical frequency comb technologies," Nat. Photonics **16**, 95–108 (2022).
18. X. Lu, S. Rogers, W. C. Jiang, and Q. Lin, "Selective engineering of cavity resonance for frequency matching in optical parametric processes," Appl. Phys. Lett. **105**, 151104 (2014).
19. X. Lu, A. Chanana, F. Zhou, M. Davanco, and K. Srinivasan, "Kerr optical parametric oscillation in a photonic crystal microring for accessing the infrared," Opt. Lett. **47**, 3331–3334 (2022).
20. J. A. Black, G. Brodnik, H. Liu, S.-P. Yu, D. R. Carlson, J. Zang, T. C. Briles, and S. B. Papp, "Optical-parametric oscillation in photonic-crystal ring resonators," Optica **9**, 1183–1189 (2022).
21. J. R. Stone, X. Lu, G. Moille, D. Westly, T. Rahman, and K. Srinivasan, "Wavelength-accurate nonlinear conversion through wavenumber selectivity in photonic crystal resonators," arXiv, arXiv:2212.05695 (2023).
22. S.-P. Yu, D. C. Cole, H. Jung, G. T. Moille, K. Srinivasan, and S. B. Papp, "Spontaneous pulse formation in edge-less photonic crystal resonators," Nat. Photonics **15**, 461–467 (2020).
23. X. Lu, A. Rao, G. Moille, D. A. Westly, and K. Srinivasan, "Universal frequency engineering tool for microcavity nonlinear optics: multiple selective mode splitting of whispering-gallery resonances," Photonics Res. **8**, 1676–1686 (2020).
24. G. Moille, X. Lu, J. Stone, D. Westly, and K. Srinivasan, "Fourier synthesis dispersion engineering of photonic crystal microrings for broadband frequency combs," Commun. Phys. **6**, 144 (2023).
25. E. Lucas, S.-P. Yu, T. C. Briles, D. R. Carlson, and S. B. Papp, "Tailoring microcombs with inverse-designed, meta-dispersion microresonators," Nat. Photonics (2023).
26. K. Y. Yang, C. Shirpurkar, A. D. White, J. Zang, L. Chang, F. Ashtiani, M. A. Guidry, D. M. Lukin, S. V. Pericherla, J. Yang, H. Kwon, J. Lu, G. H. Ahn, K. Van Gasse, Y. Jin, S.-P. Yu, T. C. Briles, J. R. Stone, D. R. Carlson, H. Song, K. Zou, H. Zhou, K. Pang, H. Hao, L. Trask, M. Li, A. Netherton, L. Rechtman, J. S. Stone, J. L. Skarda, L. Su, D. Vercruysse, J.-P. W. MacLean, S. Aghaeimeibodi, M.-J. Li, D. A. B. Miller, D. M. Marom, A. E. Willner, J. E. Bowers, S. B. Papp, P. J. Delfyett, F. Aflatouni, and J. Vučković, "Multi-dimensional data transmission using inverse-designed silicon photonics and microcombs," Nat. Commun. **13**, 7862 (2022).
27. R. Kashyap, *Fiber Bragg Gratings* (Academic, 1999).
28. K. Nozaki, A. Nakagawa, D. Sano, and T. Baba, "Ultralow threshold and single-mode lasing in microgear lasers and its fusion with quasi-periodic photonic crystals," IEEE J. Sel. Top. Quantum Electron. **9**, 1355–1360 (2003).
29. A. Arbabi, S. M. Kamali, E. Arbabi, B. G. Griffin, and L. L. Goddard, "Grating integrated single mode microring laser," Opt. Express **23**, 5335–5347 (2015).
30. R. Cheng, N. A. F. Jaeger, and L. Chrostowski, "Fully tailorable integrated-optic resonators based on chirped waveguide Moiré gratings," Optica **7**, 647–657 (2020).
31. X. Lu, M. Wang, F. Zhou, M. Heuck, W. Zhu, V. A. Aksyuk, D. R. Englund, and K. Srinivasan, "Highly-twisted states of light from a high quality factor photonic crystal ring," Nat. Commun. **14**, 1119 (2023).
32. B. Chen, Y. Zhou, P. Huang, C. Ye, Q. Cao, Y. Liu, C. Kim, K. Yvind, J. Li, C. Dong, S. Fu, Q. Zhan, X. Wang, M. Pu, and J. Liu, "Integrated optical vortex microcomb," arXiv, arXiv:2212.07641 (2023).
33. Y. Liu, C. Lao, M. Wang, Y. Cheng, S. Fu, C. Gao, J. Wang, B.-B. Li, Q. Gong, Y.-F. Xiao, W. Liu, and Q.-F. Yang, "Integrated vortex soliton microcombs," arXiv, arXiv:2212.07639 (2023).
34. X. Lu, A. McClung, and K. Srinivasan, "High-Q slow light and its localization in a photonic crystal microring," Nat. Photonics **16**, 66–71 (2022).
35. M. Wang, F. Zhou, X. Lu, A. McClung, M. Davanco, V. A. Aksyuk, and K. Srinivasan, "Fractional optical angular momentum and multi-defect-mediated mode renormalization and orientation control in photonic crystal microring resonators," Phys. Rev. Lett. **129**, 186101 (2022).

36. S. G. Johnson, M. Ibanescu, M. A. Skorobogatiy, O. Weisberg, J. D. Joannopoulos, and Y. Fink, "Perturbation theory for Maxwell's equations with shifting material boundaries," Phys. Rev. E **65**, 066611 (2002).
37. X. Lu, A. Chanana, A. McClung, Y. Sun, M. Davanco, and K. Srinivasan, Department of Electrical and Computer Engineering, University of Massachusetts Amherst, Amherst, MA 01003, USA, are preparing a manuscript to be titled "Band flipping and bandgap closing in a photonic crystal ring and its applications."
38. X. Lu, Q. Li, D. A. Westly, G. Moille, A. Singh, V. Anant, and K. Srinivasan, "Chip-integrated visible-telecom photon pair sources for quantum communication," Nat. Phys. **15**, 373–381 (2019).
39. M. H. P. Pfeiffer, C. Herkommer, J. Liu, T. Morais, M. Zervas, M. Geiselmann, and T. J. Kippenberg, "Photonic damascene process for low-loss, high-confinement silicon nitride waveguides," IEEE J. Sel. Top. Quantum Electron. **24**, 6101411 (2018).
40. A. Graf, S. D. Rogers, J. Staffa, U. A. Javid, D. H. Griffith, and Q. Lin, "Nonreciprocity in photon pair correlations of classically reciprocal systems," Phys. Rev. Lett. **128**, 213605 (2022).
41. Q. Li, M. Davanço, and K. Srinivasan, "Efficient and low-noise single-photon-level frequency conversion interfaces using silicon nanophotonics," Nat. Photonics **10**, 406–414 (2016).
42. A. E. Ulanov, T. Wildi, N. G. Pavlov, J. D. Jost, M. Karpov, and T. Herr, "Synthetic-reflection self-injection-locked microcombs," arXiv, arXiv:2301.13132 (2023).
43. F. Zhou, X. Lu, A. Rao, J. Stone, G. Moille, E. Perez, D. Westly, and K. Srinivasan, "Hybrid-mode-family Kerr optical parametric oscillation for robust coherent light generation on chip," Laser Photonics Rev. **16**, 2100582 (2022).
44. E. F. Perez, G. Moille, X. Lu, J. Stone, F. Zhou, and K. Srinivasan, "High-performance Kerr microresonator optical parametric oscillator on a silicon chip," Nat. Commun. **14**, 242 (2023).